ACS Energy LETTERS

http://pubs.acs.org/journal/aelccp

4 V Na Solid State Batteries Enabled by a Scalable Sodium Metal Oxyhalide Solid Electrolyte

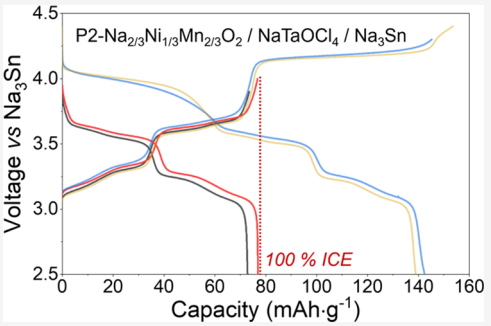
Laidong Zhou, J. David Bazak, Chang Li, and Linda F. Nazar*

Cite This: *ACS Energy Lett.* 2024, 9, 4093−4101

Read Online

ACCESS | Metrics & More | Article Recommendations | Supporting Information

ABSTRACT: **All-solid-state sodium batteries (ASSSBs) are viable candidates for large scale energy storage that could vie with lithium. Ductile solid catholytes for such cells that can be prepared without extensive ball milling and directly paired with high voltage sodium cathodes are lacking, however. We report a new amorphous fast Na-ion conducting metal oxychloride that meets these criteria, synthesized through a scalable and low-cost route based on a spontaneous solid-state reaction with simple short mixing and 100 °C annealing. It has an ionic conductivity of 1.2 mS·cm^{-1} and low activation energy of 0.31 eV. Due to its dual O^{2-}/Cl^{-} framework, it exhibits a high anodic potential of 4 V vs Na^{+}/Na and good chemical/electrochemical compatibility with high voltage sodium cathode materials. ASSSBs consisting of the oxychloride solid electrolyte paired with a high voltage P2−$Na_{2/3}Ni_{1/3}Mn_{2/3}O_2$ cathode showed stable long-term cycling with a 4.0 V vs Na_3Sn cutoff potential and even to 4.3 V.**

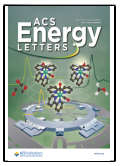


With significantly growing global commitments and action on decarbonization, increasing the use of renewable energy resources can substantially reduce the worldwide energy dependence on fossil fuels. Energy storage devices such as rechargeable batteries are needed to complement intermittent clean energy resources and can electrify transportation.[1,2] Lithium-ion batteries currently dominate the market, but all-solid-state lithium batteries have emerged as a promising next-generation candidate,[3] with the development of a range of Li superionic conductors.[4−6] However, the dramatically increasing demand for large scale energy storage and electric vehicles will likely lead to a rise in the price of lithium. Sodium ion batteries represent a very promising alternative due to sodium's low cost, high earth abundance and widely available resources. All-solid-state sodium batteries (ASSSBs) can also offer improved energy density and better safety than their liquid electrolyte analogues, as in the case of lithium.[7]

Inorganic solid electrolytes (SEs) are the key component to realize the promise of ASSSBs. Inorganic Na SEs, including oxides and sulfides, have been well-studied.[8] Oxides (NASICON-structured phases, β-alumina) and sulfides (*e.g.* $Na_{2.88}Sb_{0.86}W_{0.11}S_4$) generally exhibit the highest Na ion conductivities, comparable to or even surpassing those of liquid organic electrolytes.[9−12] However, to achieve high Na ion conductivities for oxide SEs, high-temperature sintering or even hot-pressing is needed to minimize interfacial and grain boundary resistance.[9,13] Additional high-temperature sintering is needed for cathode composites to achieve sufficient interfacial contact and minimal contact resistance, which in turn can also lead to detrimental side reactions between oxide SE and cathode active material particles.[14] Sulfide Na SEs are limited by their narrow stability voltage window, which leads to chemical and electrochemical incompatibility with high voltage sodium cathodes.[15] Borohydride SEs exhibit reasonably high ionic conductivity/voltage stability and good ductility,[16] but their expensive and complex synthesis routes limit large scale production and practical application.[17] Thus, it is essential to find Na SEs with high ionic conductivity, a wide voltage stability window and good mechanical properties, and most importantly, that can be prepared through simple and scalable synthesis routes.

Chloride and oxychloride SEs are some of the suitable choices and have shown excellent performance in high voltage all-solid-state Li batteries.[18−23] Alkali metal oxyhalides are some of the newest and perhaps most promising solid state ion conductors because they are ductile, and can be used with

Received: July 8, 2024
Accepted: July 15, 2024
Published: July 25, 2024



Downloaded via CITY UNIV OF HONG KONG on August 23, 2025 at 12:16:03 (UTC).
See https://pubs.acs.org/sharingguidelines for options on how to legitimately share published articles.

ACS Publications © 2024 American Chemical Society

https://doi.org/10.1021/acsenergylett.4c01855
ACS Energy Lett. 2024, 9, 4093−4101

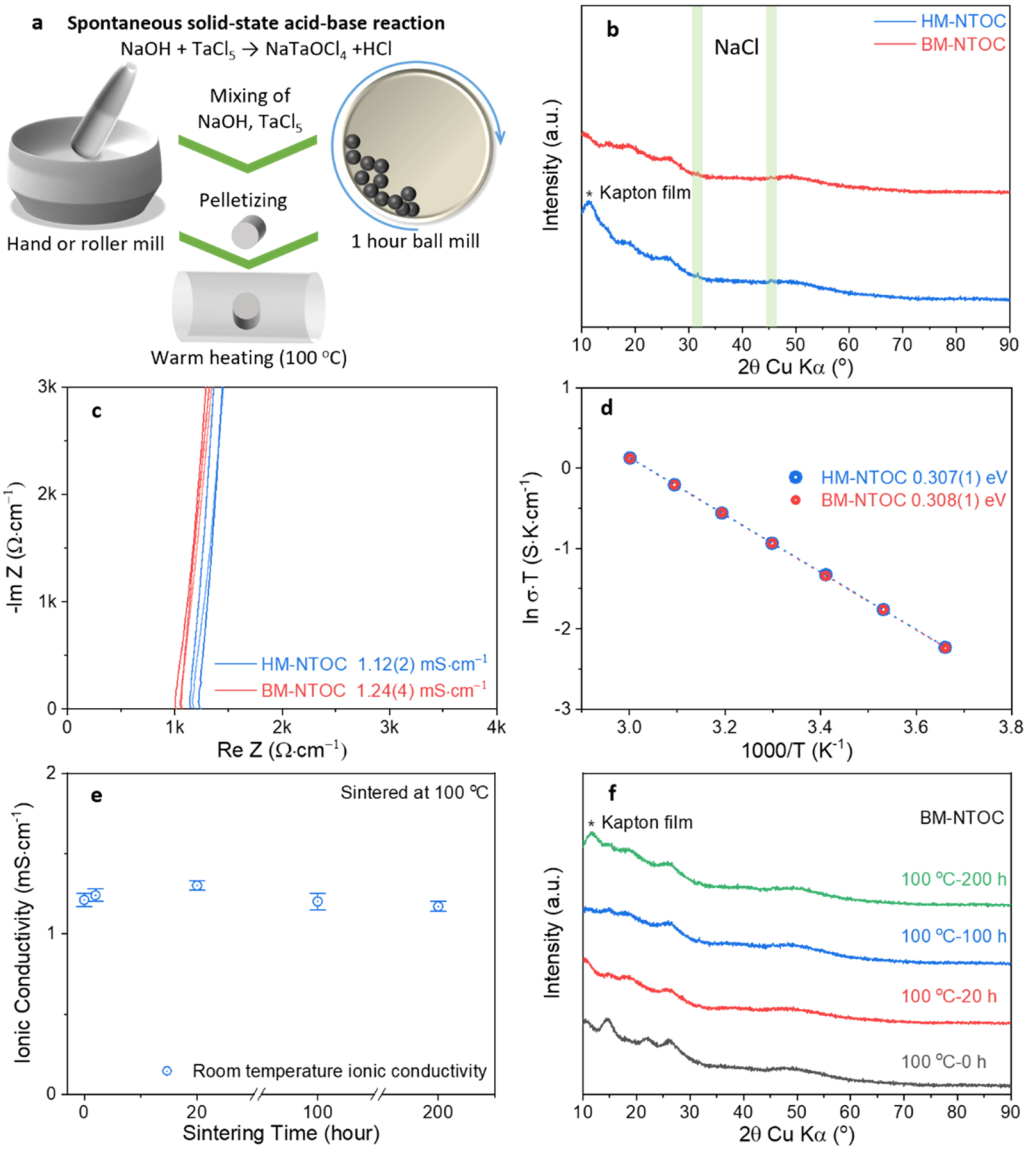


Figure 1. (a) Schematic illustration of the two routes to form $NaTaOCl_4$: hand-mixing and short-period ball-milling; (b) XRD patterns of hand-mixed (HM-NTOC) and ball-milled (BM-NTOC) synthesized $NaTaOCl_4$ with 2 h sintering at 100 °C, almost undectable NaCl peaks are shaded in green; (c) room temperature Nyquist plots of HM-NTOC and BM-NTOC, both samples were measured three times to ensure reproducibility; (d) Arrhenius plots of the conductivity values for HM-NTOC and BM-NTOC in the temperature range from 0 to 60 °C; (e) room temperature ionic conductivity variation vs sintering time at 100 °C and (f) corresponding XRD patterns. The background contribution from the zero-background Si holder and Kapton film (*) for all patterns were not subtracted, because the main phase only exhibits extremely broad peaks.

cathode-active materials without a coating on the cathode surface. In this respect, they are like their halide counterparts, but more ionically conductive. In contrast to lithium, a limited number of sodium chloride and oxychloride SEs have been reported.[24−34] The majority exhibit low ionic conductivities of <0.1 mS·cm^{-1} and/or require long-duration high energy ball-milling steps for their preparation. This cannot meet practical application requirements for large scale production.[24−31] Most recently, an interesting material, $(Li/Na)AlCl_{2.5}O_{0.75}$, was reported with a high total ionic conductivity of 1.5/1.3 mS·cm^{-1} and nonunity Li^+/Na^+ transference number.[35] When directly paired with a high voltage Li cathode - NMC622 - a notable fraction of Al_2O_3 was formed upon cell cycling, and DFT calculations suggested that the material decomposes into Al_2O_3 and $LiAlCl_4$ when oxidized.

Here, we report a new amorphous-glassy fast Na-ion conducting oxychloride, $NaTaOCl_4$, which exhibits a high ionic conductivity of 1.1 mS·cm^{-1} and a low activation energy. Most importantly, it can be synthesized through a spontaneous solid-state acid−base reaction with easy mixing and mild-temperature processing. Such a simple synthesis route is easily scalable and compatible with current industrial inorganic material synthesis processes. Furthermore, $NaTaOCl_4$ demonstrates excellent chemical and electrochemical compatibility with uncoated high voltage sodium metal oxide cathode materials. ASSSBs comprised of the $NaTaOCl_4$ SE paired with a high voltage P2−$Na_{2/3}Ni_{1/3}Mn_{2/3}O_2$ cathode show stable long-term cycling behavior over 200 cycles with a 4.0 V vs Na^+/Na cutoff voltage.

$NaTaOCl_4$ (NTOC) was synthesized by hand mixing of NaOH and $TaCl_5$ to trigger a spontaneous solid-state acid−

https://doi.org/10.1021/acsenergylett.4c01855
ACS Energy Lett. 2024, 9, 4093−4101

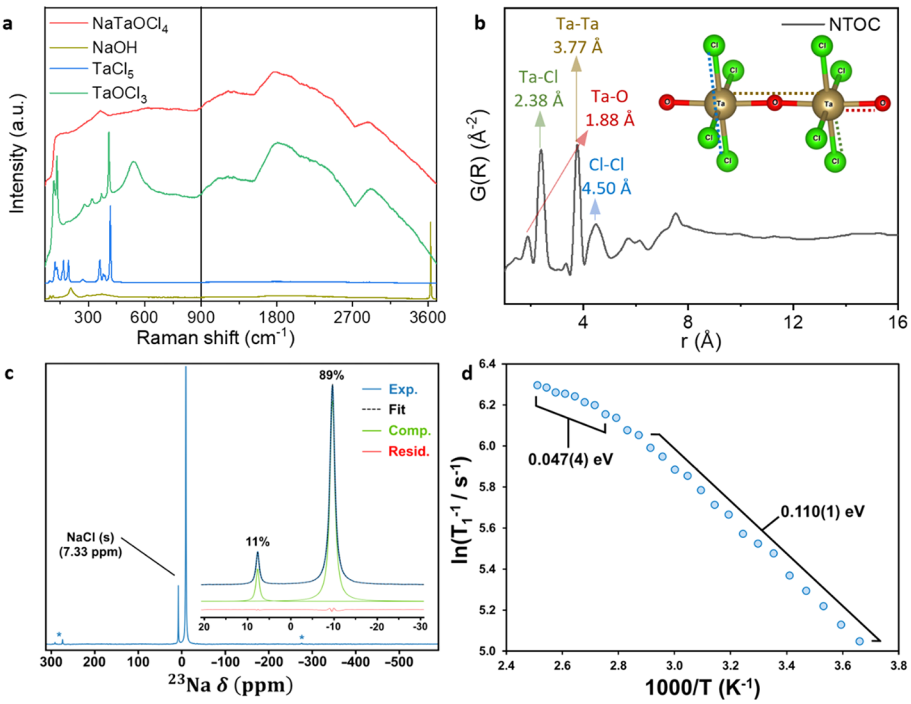


Figure 2. (a) Raman spectra of amorphous $NaTaOCl_4$ and crystalline NaOH, $TaCl_5$ and $TaOCl_3$; (b) pair distribution function analysis of synchrotron X-ray total scattering data for amorphous $NaTaOCl_4$ at 300 K; (c) ^{23}Na 60 kHz MAS spectrum at 280 K (asterisks denote spinning side-bands; inset provides deconvolution and signal integrations) and (d) Arrhenius plot of static ^{23}Na T_1 relaxation measurements.

base reaction, followed by heating this mixture at 100 °C for 2 h to ensure complete reaction and remove any remaining HCl (Figure 1a). The corresponding XRD pattern of the hand-mixed $NaTaOCl_4$, denoted as HM-NTOC, showed no significant diffraction peaks with only remarkably broad and low intensity peaks centered at around 15°, 19° and 26°, indicating its amorphous-glassy nature (Figure 1b). The high background at low angle is due to scattering from the zero-background Si holder and Kapton film (Figure S1) used to avoid sample exposure to air. HM-NTOC exhibited a high Na^+ conductivity of 1.1 mS·cm^{-1} and a low activation energy of 0.31 eV (Figures 1c-d, S2a, Table S1). The time required for thorough mixing to ensure full amorphization may differ based on the operator (Figure S3), while roller mills could be employed for large-scale production. To standardize the synthesis, $NaTaOCl_4$ was also synthesized through a short 1 h ball-mill period followed by the same 100 °C heat-treatment for 2 h (Figure 1a). The corresponding XRD pattern of ball-milled $NaTaOCl_4$ (denoted as BM-NTOC) showed the same amorphous-glassy nature as HM-NTOC with the same broad peaks at ∼15°, 19° and 26° (Figure 1b). BM-NTOC also exhibited nearly the same ionic conductivity of 1.2 mS·cm^{-1} and activation energy of 0.31 eV (Figures 1c-d, S2b, Table S1). This preparation route is also applicable to $NaNbOCl_4$ (NNOC), which can be synthesized through both hand-mixing and brief ball-milling, although a semicrystalline material was obtained for NNOC. Furthermore, HM-NNOC contained slightly more NaCl impurity than BM-NNOC (Figure S4a), while NNOC exhibited a lower ionic conductivity of ∼0.5 mS·cm^{-1} and a higher activation energy of 0.34 eV (Figure S4b-e, Table S2). The SEM images of NTOC and NNOC (Figure S5) revealed micron-sized particles in both hand-mixed and ball-milled samples, although the particle size and morphology of the as-synthesized solid electrolytes depend on the final grinding step.

One important consideration for glassy/amorphous SE materials is their thermal stability. During cell charging, temperature increases are generally observed,[36,37] and elevated-temperature heating is often used to realize fast charging for commercial Li-ion batteries.[38,39] However, amorphous materials may crystallize at moderate temperatures which can lead to dramatically lower ionic conductivity.[24,28] Since cell temperatures are typically maintained below 100 °C to ensure safety and keep costs low, the thermal stability of NTOC was examined by annealing at that temperature for different periods, during which the ionic conductivity remained nearly constant up to 200 h (Figures 1e, S6). The XRD patterns of annealed samples (Figure 1f) revealed that its amorphous-glassy nature also was maintained over this annealing period, with the same extremely broad and low intensity peaks centered at around 15°, 19° and 26°. The XRD pattern of the BM sample without annealing shows slightly better-defined broad peaks; however, due to their very limited number, it is not possible to identify the possible nanocrystalline phase.

The Raman spectrum of NTOC (Figure 2a) reveals that no starting material ($TaCl_5$ or NaOH) remains. NTOC exhibits similar features as crystalline $TaOCl_3$, with the characteristic sharp peaks of the latter becoming very broad peaks in $NaTaOCl_4$. This is strong evidence of its amorphous disordered structure. The Raman spectrum of the analogous Nb oxychloride glass-ceramic (NNOC; $NaNbOCl_4$) also showed characteristic peaks of crystalline $NbOCl_3$ (Figure S7). This suggests that $TaCl_5$/$NbCl_5$ reacts with NaOH to form chains of oxygen corner-sharing $(Ta/Nb)O_2Cl_4$ octahedral moieties (Figure 2b inset), similar to $TaOCl_3$, but with Na^+ randomly distributed within the matrix.[22] We note that we

https://doi.org/10.1021/acsenergylett.4c01855
ACS Energy Lett. 2024, 9, 4093−4101

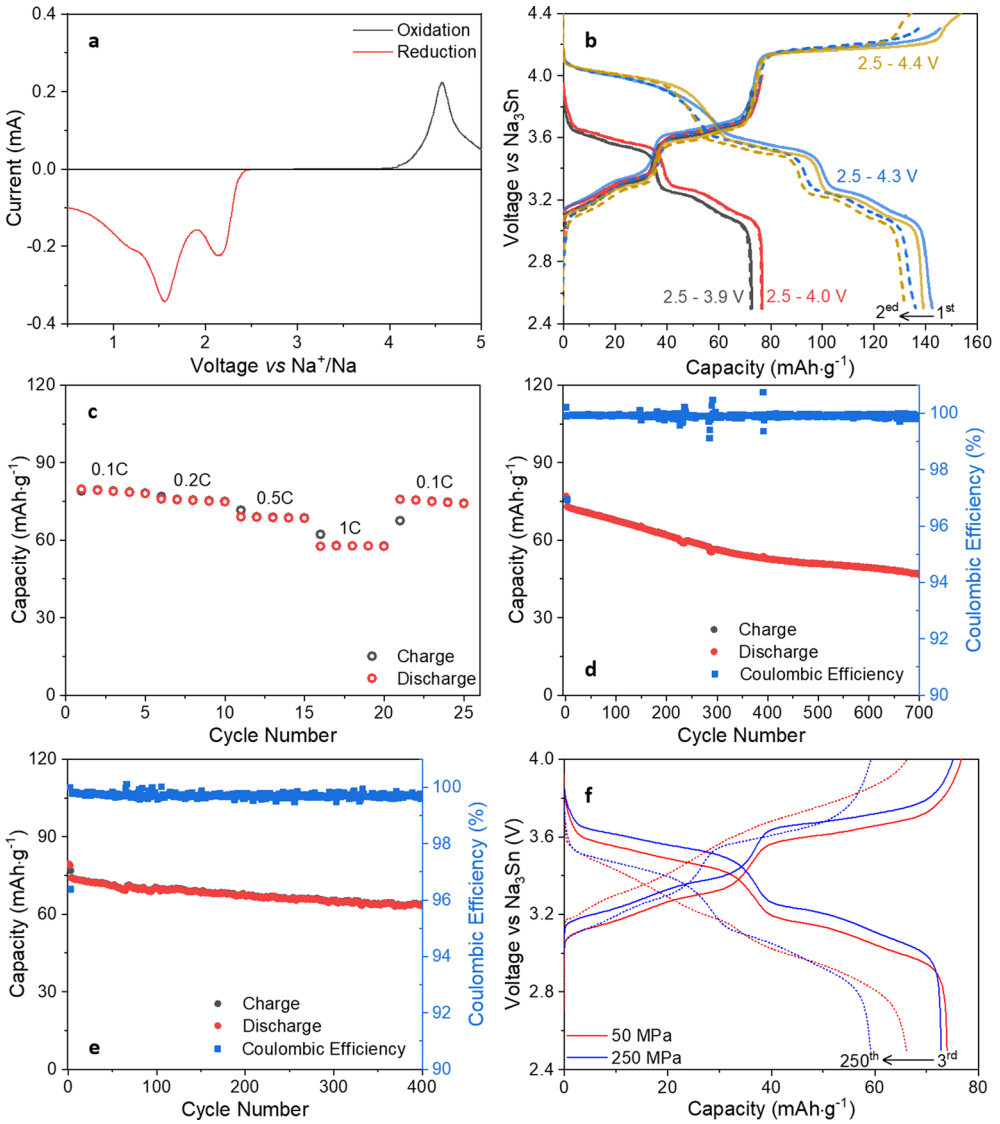


Figure 3. (a) Linear sweep voltammograms at a scan rate of 0.1 mV·s^{-1} with a Na metal anode and a NTOC/Super P carbon (90:10 wt %) composite cathode; two cells were fabricated for the cathodic and anodic scans, respectively; (b) voltage profile of NNMO ASSSBs at a 0.1 C rate for the initial two cycles (1st cycle in solid line and 2^{ed} cycle in dashed line) with cutoff potentials of 3.9 V, 4.0 V, 4.3 and 4.4 V vs Na_3Sn; (c) charge−discharge capacity as a function of cycle number at different C rates for NNMO ASSSB with NTOC and a Na_2Sn anode; long-term cycling performance of NNMO ASSSBs with 4.0 V vs Na_3Sn cutoff potentials at different applied pressure (d) 250 MPa and (e) 50 MPa and the corresponding voltage profiles (f). The first two cycles were conducted at a 0.1 C rate followed by a C/3 rate. The composite cathode consisted of NNMO-NTOC-Super P carbon (67:30:3 wt.%); NTOC and $Na_4(CB_{11}H_{12})_2(B_{12}H_{12})$ were used as the solid electrolyte layer facing counter electrode and reference electrode, respectively.

determined such building blocks - consisting of 1-D $[NbOCl_4]^-$ anionic chains linked by Nb−O−Nb bonds and separated by multiple, disordered Li^+ sites - exist in semicrystalline $LiNbOCl_4$ on the basis of fitting its X-ray and neutron pair distribution function (PDF).[40] However, the fully amorphous nature of $NaTaOCl_4$ precludes generating a definitive model. The X-ray PDF of $NaTaOCl_4$ (Figure 2b) consists of two unique segments, with similar well-defined features at $r < 8$ Å indicating the local structure and interplay of the main building blocks. For $r > 8$ Å the PDF becomes featureless, indicating its glassy nature with no long-range ordering (and prohibiting detailed analysis). Due to the low content of Na along with dominant-diffracting heavier elements, the PDF data shows only clear contributions from Ta−O, Ta−Cl, Ta−Ta and Cl−Cl (Figure 2b, as labeled). The contribution of Na (i.e., Na−Cl at 2.8 Å) is not distinguishable. Nonetheless, the distances of Ta−Cl (2.38 Å), Ta−O (1.88 Å) and Ta−Ta (3.77 Å) agree well with those of crystalline $TaOCl_3$, and also mirror those of $LiNbOCl_4$ (Nb−Cl; avg. 2.41 Å), Nb−O (1.76 Å/2.25 Å) and Nb−Nb (3.75 Å).[40] This supports our local structural model.

A ^{23}Na 60 kHz magic-angle-spinning (MAS) solid-state NMR spectrum performed on $NaTaOCl_4$ at 280 K exhibited two peaks (Figure 2c). The main peak (at −10 ppm) corresponds to the primary $NaTaOCl_4$ phase and the minor peak at 7.33 ppm corresponds to a NaCl signal,[24,41] which has a ^{23}Na chemical shift of ∼7.1 ppm. Peak deconvolution yielded a molar ratio of $NaCl/NaTaOCl_4$ of ∼1/8, which corresponds to only 2 wt % NaCl impurity, in agreement with its negligible contribution in the XRD pattern (Figure 1b). Such a low content of NaCl will be embedded in the amorphous $NaTaOCl_4$ matrix and obviously will not lower its ionic

https://doi.org/10.1021/acsenergylett.4c01855
ACS Energy Lett. 2024, 9, 4093−4101

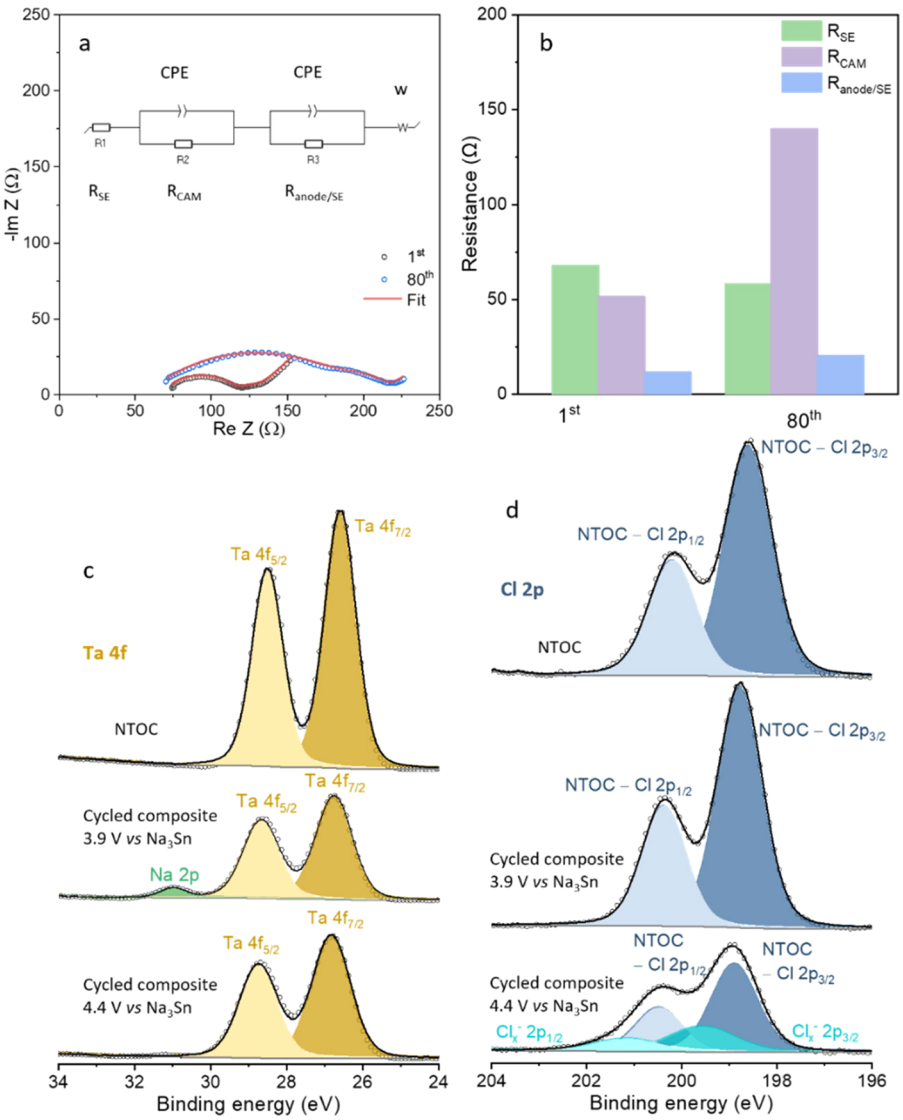


Figure 4. (a) Nyquist plots and the corresponding fit of the NNMO ASSSB at the initial and 80th charge to 3.5 V vs Na_3Sn; the inset is the equivalent circuit used to fit the EIS data; (b) summary of the fitting results; (c) Ta 4f and (d) Cl 2p XPS spectra of pristine NTOC and cycled composite cathodes with 3.9 and 4.4 V vs Na_3Sn cutoff potentials, the spin doublet components are shaded with the same color for each spectrum. The XPS peaks of cycled composites shifted to higher binding energy by ~0.2 eV compared to bare pristine NTOC, which is attributed to the effect of mixing conducting cathode active material and carbon. The XPS spectra for the same element are on the same intensity scale.

conductivity. Notably, there was only a single, miniscule spinning sideband for the main $NaTaOCl_4$ phase, and the central transition signal can be very well fit by a single Lorentzian component, which indicates motional narrowing owing to the high mobility of the Na ions.[42] For an amorphous Na-containing material without motional averaging of the line shape by diffusion, a distribution of quadrupolar couplings would be expected, which would significantly broaden the central transition.[43]

To further elucidate the Na^+ local motional dynamics, static ^{23}Na saturation recovery measurements of the longitudinal relaxation rate, T_1, were performed as a function of temperature. The resulting Arrhenius plot (Figure 2d) demonstrates a low activation energy of 0.110 eV over the temperature range extending from 273 K to approximately 353 K, which indicates fast Na^+ local motion comparable with what has been measured using this technique for Ga-doped layered $Na_2Zn_2TeO_6$ and Na-doped $SrSiO_3$,[44,45] and half of what has been reported for Na_3PS_4, $Na_3B_5S_9$ and NASICON-type $Na_{3.4}Sc_2(SiO_4)_{0.4}(PO_4)_{2.6}$.[46−48] Interestingly, above 353 K and to the maximum temperature that the magnet shim can withstand (398 K), there is a marked inflection in the Arrhenius plot, and a significantly lower-activation relaxation process begins to dominate. Correspondingly, there is a considerable shift in the 7.33 ppm peak position toward the primary (−10 ppm) signal and concomitant broadening of both signals (Figure S8) indicative of exchange approaching a coalescence point.[42] This implies that the ion conduction mechanism begins to change above 353 K and there is increased participation from the NaCl population, potentially indicating that NaCl could be defective and become exchangeable at elevated temperatures.

The stability voltage range of $NaTaOCl_4$ measured with linear sweep voltammetry (LSV) (Figure 3a) demonstrates a high oxidation potential of 4.0 V vs Na^+/Na determined by the Cl^- anion framework. The reduction potential is 2.45 V vs

https://doi.org/10.1021/acsenergylett.4c01855
ACS Energy Lett. 2024, 9, 4093−4101

Na^+/Na as dictated by Ta^{5+} reduction. Taking its electrochemical stability window into consideration, P2-type $Na_{2/3}Ni_{1/3}Mn_{2/3}O_2$ (NNMO) was chosen as the high voltage cathode to demonstrate NTOC's electrochemical properties. Phase-pure micron-sized NNMO (Figure S9) was synthesized following previously reported procedures.[49] Using an uncoated NNMO positive electrode and a Na_3Sn/Na_2Sn negative electrode, ASSSBs were fabricated. The sloping reference potentials of Na_3Sn and Na_2Sn are about ~0.10 and 0.14 V vs Na^+/Na respectively (Figure S10). A thin layer of $Na_4(CB_{11}H_{12})_2(B_{12}H_{12})$ (Figure S11) was used to separate NTOC from Na_3Sn/Na_2Sn to prevent its reduction.[16] The cathode composite consisted of 67 wt % NNMO, 30 wt % NTOC and 3 wt % Super P carbon with a moderate cathode loading of ~9 $mg_{NNMO}\cdot cm^{-2}$. Even though the as-synthesized NTOC comprises micron-sized large particles, after initial cathode composite mixing, the SEM images and energy-dispersive X-ray spectroscopy (EDX) maps (Figure S12) show that NTOC is well distributed and forms a semiuniform thin SE coating on the NNMO, due to its relatively soft nature. Such a semiuniform coating and addition of conductive super P carbon enable Li-ion and electron percolation within the cathode composite. ASSSBs were cycled with different cutoff potentials of 3.9 V, 4.0 V, 4.3 and 4.4 V vs Na_3Sn at room temperature (Figure 3b). At a 0.1 C rate, a 100% initial Coulombic efficiency (ICE) was achieved for cells cycled to 3.9 and 4.0 V vs Na_3Sn, and the cell cycled to 4.3 V also exhibited a high ICE of 98%. This highlights the intrinsically high oxidation stability of NTOC and its good chemical and electrochemical stability with high voltage cathodes. Only upon cycling the cell to 4.4 V vs Na_3Sn was a lower ICE of 90.5% obtained, (partially due to the oxidation of NTOC) which led to increased cell internal resistance and thus lower discharge capacity. Cross-sectional SEM images (Figure S13) demonstrate that the NNMO particles maintained good contact with NTOC SE after multiple cycles. Na_2Sn was used as an anode material instead of Na_3Sn for rate cycling to avoid dendrite growth at high current densities, and showed excellent rate capability for the NNMO ASSSB (Figures 3c, S14a).

The NTOC ASSSBs also exhibited good cycling stability using upper cutoff potentials of 4.0 and 4.3 V vs Na_3Sn (Figures 3d, S14b-c). With a 4.0 V cutoff potential, only $Ni^{2+/3+}$ redox is active. However, increase to a 4.3 V cutoff potential leads to $Ni^{3+/4+}$ and oxygen redox activity, along with a phase transformation from P2 to O2 and a large volume shrinkage (~23%), which leads to faster capacity fading for both liquid and solid state cells.[50,51] While within the stability voltage window of NTOC, cells cycled below 4.0 V still exhibit gradual capacity fading, which could be attributed to mechanical effects. When NNMO is charged to 4.0 V, only 1/3 Na^+ is extracted, leading to a low (~1.25%) volume expansion.[52] Thus, the cathode composite will not suffer from dramatic volume changes during Na^+ deintercalation/insertion. However, the Na−Sn alloy anode does exhibit a large volume expansion of 25% on Na insertion from Na_3Sn to $Na_{15}Sn_4$ upon charging.[53] During extensive cell cycling, repeated volume expansion and extraction of the Na−Sn anode together with the high applied external pressure will lead to dynamic strain and release within the entire cell, gradually degrading the cell materials and lowering the capacity. Fortuitously, with a much lower applied pressure of 50 MPa, ASSSB (Figure 3e, f) showed the same initial discharge capacity but better capacity retention of 89.5% than the 82.0% provided for cells cycled under 50 MPa pressure over 250 cycles (Figure 3d).

To further demonstrate the chemical and electrochemical stability of NTOC with NNMO, EIS measurements were conducted after the cell was first charged to 3.5 V vs Na_3Sn and then cycled between 2.5 to 4.0 V for over 80 cycles, stopping at each cycle at 3.5 V for the EIS measurement (Figure S15). The cell internal resistance increased between the initial impedance and that recorded after the 80th cycle (Figure 4a). The fitting results are summarized in Figure 4b (the equivalent circuit model is shown in the inset of Figure 4a): R_{SE} represents the bulk SE separator resistance, which decreased from 67.7 Ω to 58.2 Ω due to consolidation during long-term cycling.[54,55] The cathode composite resistance (R_{CAM}) was 51.4 Ω after the initial charge to 3.5 V, and increased to 140 Ω after the 80th charge. However, the charge transport and charge transfer within the cathode that includes ionic, electronic, and interfacial contributions cannot be separated. The overall cathode resistance increase could be attributed to the electrochemical oxidation of NTOC, a chemical reaction between NTOC and NNMO, Na^+ diffusivity variation of NNMO at different desodiation degrees,[56] or contact loss between NTOC-NNMO due to cell volume changes after extensive cycling. The 100% ICE (Figure S15) does prove NTOC's high oxidation stability and chemical compatibility with NNMO when charged to only 4.0 V vs Na_3Sn. Owing to the increased cell internal resistance, the cell charged to 3.5 V at its 80th cycle deintercalated less Na^+ from NNMO compared to the initial charge due to higher overpotential and volume changes from the Na_3Sn anode that further led to increased charge transfer resistance within the cathode composite. The anode interfacial resistance ($R_{anode/SE}$) also almost doubled from 11.6 Ω to 20.4 Ω (Figure 4b). As $Na_4(CB_{11}H_{12})_2(B_{12}H_{12})$ is stable with Na metal,[16] the increase in $R_{anode/SE}$ is also due to the volume change of Na_3Sn during cycling, which gradually pulverizes the $Na_4(CB_{11}H_{12})_2(B_{12}H_{12})/Na_3Sn$ interfacial layer. This can be attributed as another main reason for capacity fading.

Ex situ X-ray photoelectron spectroscopy (XPS) analysis was further conducted to determine the nature of the possible degradation products between NTOC and NNMO. Cells were first cycled at a 0.1 C rate for 10 cycles with 3.9 and 4.4 V vs Na_3Sn cutoff potentials (Figure S16), then XPS measurements were conducted at the discharged stage on the top surface of the cathode composites. The Ta 4*f* XPS spectra (Figure 4c) exhibits no obvious changes after cycling to 4.4 V compared to pristine NTOC. A small Na 2*p* signal was observed only for the cell cycled to 3.9 V. The Cl 2*p* spectra (Figure 4d) displayed no noticeable change between pristine NTOC and the sample cycled to 3.9 V. However, when cycled to 4.4 V, Cl 2*p* spectra exhibited new peaks at higher binding energy, indicating the presence of oxidation products of Cl_x^-, corresponding to the electrochemical degradation of oxychloride SE.[57] However, these results confirm the high oxidation and chemical and electrochemical stability of NTOC with high voltage cathodes up to 4.0 V vs Na^+/Na.

In summary, we present a sodium fast ion conductor oxychloride - $NaTaOCl_4$ - synthesized by a gentle mechanically initiated reaction without requiring long-duration high energy ball-milling or high temperature sintering. In contrast, initial reports of $LiTaOCl_4$ cited the need for 30−40 h of mechanochemical synthesis which is not commercially viable.[20,21] Amorphous $NaTaOCl_4$ exhibits a high ionic

https://doi.org/10.1021/acsenergylett.4c01855
ACS Energy Lett. 2024, 9, 4093−4101

conductivity of 1.2 mS·cm^{-1} and a low activation energy of 0.31 eV. Solid-state ^{23}Na NMR confirms fast Na^+ local motion. Excellent chemical and electrochemical stability between NTOC and NNMO are observed on cycling up to 4.0 V vs Na_3Sn. Even with a 4.3 V vs Na_3Sn cutoff potential, ASSSB still sustains relatively stable cycling. XPS and EIS analysis revealed the presence of a clean NNMO/NTOC interface up to a cutoff potential of 4.0 V vs Na^+/Na. Overall, this work demonstrates metal oxychloride Na^+-ion conductors are promising SEs for all solid-state sodium batteries and can be synthesized through a spontaneous acid−base reaction with simple mixing allowing for mass production. This approach could be also applied to other reported oxychloride SEs.[22,35] Nearly all halide solid electrolytes are based on rare-earth or rare metals, so future work should also focus on cost-effective and environmentally friendly solutions for recycling ASSBs to recover these rare-earth or rare metals and to lower the cost of ASSBs and achieve a circular economy.[58]

■ ASSOCIATED CONTENT

Data Availability Statement

Data generated and analyzed in this study are included in the paper and Supporting Information.

Supporting Information

The Supporting Information is available free of charge at https://pubs.acs.org/doi/10.1021/acsenergylett.4c01855.

Experimental methods, Nyquist plots, electrochemical data, SEM (PDF)

■ AUTHOR INFORMATION

Corresponding Author

Linda F. Nazar − *Department of Chemistry and the Waterloo Institute for Nanotechnology, University of Waterloo, Waterloo, ON N2L 3G1, Canada; Joint Center for Energy Storage Research, Argonne National Laboratory, Lemont, Illinois 60439, United States;* orcid.org/0000-0002-3314-8197; Email: lfnazar@uwaterloo.ca

Authors

Laidong Zhou − *Department of Chemistry and the Waterloo Institute for Nanotechnology, University of Waterloo, Waterloo, ON N2L 3G1, Canada; Joint Center for Energy Storage Research, Argonne National Laboratory, Lemont, Illinois 60439, United States;* orcid.org/0000-0002-8556-3296

J. David Bazak − *Joint Center for Energy Storage Research, Argonne National Laboratory, Lemont, Illinois 60439, United States; Physical & Computational Science Directorate, Pacific Northwest National Laboratory, Richland, Washington 99354, United States;* orcid.org/0000-0002-4599-3208

Chang Li − *Department of Chemistry and the Waterloo Institute for Nanotechnology, University of Waterloo, Waterloo, ON N2L 3G1, Canada; Joint Center for Energy Storage Research, Argonne National Laboratory, Lemont, Illinois 60439, United States;* orcid.org/0000-0001-5420-3856

Complete contact information is available at: https://pubs.acs.org/10.1021/acsenergylett.4c01855

Author Contributions

L.Z. and L.F.N. conceived the concept and L.Z. designed and conducted the experimental work. J.D.B. performed the NMR measurements and data analysis. C.L. performed the SEM measurements and XPS data analysis. L.Z., J.D.B. and L.F.N. wrote the manuscript with input from all authors.

Notes

The authors declare no competing financial interest.

■ ACKNOWLEDGMENTS

This work was supported by the Joint Center for Energy Storage Research, an Energy Innovation Hub funded by the US Department of Energy (DOE), Office of Science, Basic Energy Sciences; and NSERC via their Canada Research Chair, Discovery Grant and the Ontario Research Fund to L.F.N. Synchrotron PDF measurements were performed using BXDS-WHE beamline at the Canadian Light Source, a national research facility of the University of Saskatchewan, which is supported by the Canada Foundation for Innovation (CFI), the Natural Sciences and Engineering Research Council (NSERC), the National Research Council (NRC), the Canadian Institutes of Health Research (CIHR), the Government of Saskatchewan, and the University of Saskatchewan. We thank Dr. Joel Reid from the CLS for the synchrotron data collection, and Dr. Peter Broderson (University of Toronto) for carrying out the XPS experiments. NMR measurements were carried out at the Pacific Northwest National Laboratory Energy Sciences Center; a portion of the NMR work was performed on a project award (10.46936/cpcy.proj.2022.60621/60008704) from the Environmental Molecular Sciences Laboratory, a DOE Office of Science User Facility sponsored by the Biological and Environmental Research program under Contract No. DE-AC05-76RL01830.

■ REFERENCES

(1) Bauer, C.; Burkhardt, S.; Dasgupta, N. P.; Ellingsen, L. A.-W.; Gaines, L. L.; Hao, H.; Hischier, R.; Hu, L.; Huang, Y.; Janek, J.; et al. Charging Sustainable Batteries. *Nat. Sustain.* **2022**, *5* (3), 176−178.

(2) Trahey, L.; Brushett, F. R.; Balsara, N. P.; Ceder, G.; Cheng, L.; Chiang, Y.-M.; Hahn, N. T.; Ingram, B. J.; Minteer, S. D.; Moore, J. S.; et al. Energy Storage Emerging: A Perspective from the Joint Center for Energy Storage Research. *Proc. Natl. Acad. Sci. U.S.A.* **2020**, *117* (23), 12550−12557.

(3) Chen, R.; Li, Q.; Yu, X.; Chen, L.; Li, H. Approaching Practically Accessible Solid-State Batteries: Stability Issues Related to Solid Electrolytes and Interfaces. *Chem. Rev.* **2020**, *120* (14), 6820−6877.

(4) Kamaya, N.; Homma, K.; Yamakawa, Y.; Hirayama, M.; Kanno, R.; Yonemura, M.; Kamiyama, T.; Kato, Y.; Hama, S.; Kawamoto, K.; et al. A lithium superionic conductor. *Nat. Mater.* **2011**, *10* (9), 682−686.

(5) Zhou, L.; Assoud, A.; Zhang, Q.; Wu, X.; Nazar, L. F. New family of argyrodite thioantimonate lithium superionic conductors. *J. Am. Chem. Soc.* **2019**, *141* (48), 19002−19013.

(6) Han, G.; Vasylenko, A.; Daniels, L. M.; Collins, C. M.; Corti, L.; Chen, R.; Niu, H.; Manning, T. D.; Antypov, D.; Dyer, M. S.; et al. Superionic lithium transport via multiple coordination environments defined by two-anion packing. *Science* **2024**, *383* (6684), 739−745.

(7) Wang, X.; Zhang, C.; Sawczyk, M.; Sun, J.; Yuan, Q.; Chen, F.; Mendes, T. C.; Howlett, P. C.; Fu, C.; Wang, Y.; et al. Ultra-Stable All-Solid-State Sodium Metal Batteries Enabled by Perfluoropolyether-Based Electrolytes. *Nat. Mater.* **2022**, *21* (9), 1057−1065.

(8) Huang, J.; Wu, K.; Xu, G.; Wu, M.; Dou, S.; Wu, C. Recent Progress and Strategic Perspectives of Inorganic Solid Electrolytes: Fundamentals, Modifications, and Applications in Sodium Metal Batteries. *Chem. Soc. Rev.* **2023**, *52* (15), 4933−4995.

(9) Ma, Q.; Tsai, C.-L.; Wei, X.-K.; Heggen, M.; Tietz, F.; Irvine, J. T. S. Room Temperature Demonstration of a Sodium Superionic Conductor with Grain Conductivity in Excess of 0.01 $S.cm^{-1}$ and Its Primary Applications in Symmetric Battery Cells. *J. Mater. Chem. A* **2019**, *7* (13), 7766−7776.
(10) Kummer, J. T. *β*-Alumina Electrolytes. *Prog. Solid State Chem.* **1972**, *7*, 141−175.
(11) Hayashi, A.; Masuzawa, N.; Yubuchi, S.; Tsuji, F.; Hotehama, C.; Sakuda, A.; Tatsumisago, M. A Sodium-Ion Sulfide Solid Electrolyte with Unprecedented Conductivity at Room Temperature. *Nat. Commun.* **2019**, *10* (1), 5266.
(12) Moon, C. K.; Lee, H. J.; Park, K. H.; Kwak, H.; Heo, J. W.; Choi, K.; Yang, H.; Kim, M. S.; Hong, S. T.; Lee, J. H.; et al. Vacancy-driven Na^+ superionic conduction in new Ca-doped Na_3PS_4 for all-solid-state Na-ion batteries. *ACS Energy Lett.* **2018**, *3* (10), 2504−2512.
(13) Valle, J. M.; Huang, C.; Tatke, D.; Wolfenstine, J.; Go, W.; Kim, Y.; Sakamoto, J. Characterization of Hot-Pressed von Alpen Type NASICON Ceramic Electrolytes. *Solid State Ionics* **2021**, *369*, 115712.
(14) Noguchi, Y.; Kobayashi, E.; Plashnitsa, L. S.; Okada, S.; Yamaki, J. Fabrication and Performances of All Solid-State Symmetric Sodium Battery Based on NASICON-Related Compounds. *Electrochim. Acta* **2013**, *101*, 59−65.
(15) Tian, Y.; Shi, T.; Richards, W. D.; Li, J.; Kim, J. C.; Bo, S.-H.; Ceder, G. Compatibility Issues between Electrodes and Electrolytes in Solid-State Batteries. *Energy Environ. Sci.* **2017**, *10* (5), 1150−1166.
(16) Asakura, R.; Reber, D.; Duchêne, L.; Payandeh, S.; Remhof, A.; Hagemann, H.; Battaglia, C. 4 V Room-Temperature All-Solid-State Sodium Battery Enabled by a Passivating Cathode/Hydroborate Solid Electrolyte Interface. *Energy Environ. Sci.* **2020**, *13* (12), 5048−5058.
(17) Duchêne, L.; Remhof, A.; Hagemann, H.; Battaglia, C. Status and Prospects of Hydroborate Electrolytes for All-Solid-State Batteries. *Energy Storage Mater.* **2020**, *25*, 782−794.
(18) Zhou, L.; Zuo, T. T.; Kwok, C. Y.; Kim, S. Y.; Assoud, A.; Zhang, Q.; Janek, J.; Nazar, L. F. High Areal Capacity, Long Cycle Life 4 V Ceramic All-Solid-State Li-Ion Batteries Enabled by Chloride Solid Electrolytes. *Nat. Energy* **2022**, *7* (1), 83−93.
(19) Li, X.; Liang, J.; Luo, J.; Banis, M. N.; Wang, C.; Li, W.; Deng, S.; Yu, C.; Zhao, F.; Hu, Y.; et al. Air-Stable Li_3InCl_6 Electrolyte with High Voltage Compatibility for All-Solid-State Batteries. *Energy Environ. Sci.* **2019**, *12* (9), 2665−2671.
(20) Ishiguro, Y.; Ueno, K.; Nishimura, S.; Iida, G.; Igarashib, Y. $TaCl_5$-Glassified Ultrafast Lithium Ion-Conductive Halide Electrolytes for High-Performance All-Solid-State Lithium Batteries. *Chem. Lett.* **2023**, *52* (4), 237−241.
(21) Asano, T.; Sakai, A.; Ouchi, S.; Sakaida, M.; Miyazaki, A.; Hasegawa, S. Solid Halide Electrolytes with High Lithium-Ion Conductivity for Application in 4 V Class Bulk-Type All-Solid-State Batteries. *Adv. Mater.* **2018**, *30* (44), 1803075.
(22) Tanaka, Y.; Ueno, K.; Mizuno, K.; Takeuchi, K.; Asano, T.; Sakai, A. New Oxyhalide Solid Electrolytes with High Lithium Ionic Conductivity > 10 $mS.cm^{-1}$ for All-Solid-State Batteries. *Angew. Chem., Int. Ed.* **2023**, *62* (13), No. e202217581.
(23) Kwak, H.; Wang, S.; Park, J.; Liu, Y.; Kim, K. T.; Choi, Y.; Mo, Y.; Jung, Y. S. Emerging halide superionic conductors for all-solid-state batteries: design, synthesis, and practical applications. *ACS Energy Lett.* **2022**, *7* (5), 1776−1805.
(24) Ridley, P.; Nguyen, L. H. B.; Sebti, E.; Han, B.; Duong, G.; Chen, Y. T.; Sayahpour, B.; Cronk, A.; Deysher, G.; Ham, S. Y.; et al. Amorphous and Nanocrystalline Halide Solid Electrolytes with Enhanced Sodium-Ion Conductivity. *Matter* **2024**, *7* (2), 485−499.
(25) Kwak, H.; Lyoo, J.; Park, J.; Han, Y.; Asakura, R.; Remhof, A.; Battaglia, C.; Kim, H.; Hong, S. T.; Jung, Y. S. Na_2ZrCl_6 Enabling Highly Stable 3 V All-Solid-State Na-Ion Batteries. *Energy Storage Mater.* **2021**, *37*, 47−54.
(26) Schlem, R.; Banik, A.; Eckardt, M.; Zobel, M.; Zeier, W. G. $Na_{3-x}Er_{1-x}Zr_xCl_6$−A Halide-Based Fast Sodium-Ion Conductor with Vacancy-Driven Ionic Transport. *ACS Appl. Energy Mater.* **2020**, *3* (10), 10164−10173.
(27) Zhao, T.; Kraft, M. A.; Zeier, W. G. Synthesis-Controlled Polymorphism and Anion Solubility in the Sodium-Ion Conductor $Na_3InCl_{6-x}Br_x$ ($0 \leq x \leq 2$). *Inorg. Chem.* **2023**, *62* (30), 11737−11745.
(28) Zhao, T.; Sobolev, A. N.; Schlem, R.; Helm, B.; Kraft, M. A.; Zeier, W. G. Synthesis-Controlled Cation Solubility in Solid Sodium Ion Conductors $Na_{2+x}Zr_{1-x}In_xCl_6$. *ACS Appl. Energy Mater.* **2023**, *6* (8), 4334−4341.
(29) Fu, J.; Wang, S.; Wu, D.; Luo, J.; Wang, C.; Liang, J.; Lin, X.; Hu, Y.; Zhang, S.; Zhao, F.; et al. Halide Heterogeneous Structure Boosting Ionic Diffusion and High-Voltage Stability of Sodium Superionic Conductors. *Adv. Mater.* **2024**, *36* (3), 2308012.
(30) Park, J.; Han, D.; Son, J. P.; Kwak, H.; Ko, W.; Park, C.; Lee, C.; Lee, H. W.; Kim, J.; Nam, K. W.; et al. Extending the Electrochemical Window of Na^+ Halide Nanocomposite Solid Electrolytes for 5 V-Class All-Solid-State Na-Ion Batteries. *ACS Energy Lett.* **2024**, *9* (5), 2222−2230.
(31) Park, J.; Son, J. P.; Ko, W.; Kim, J. S.; Choi, Y.; Kim, H.; Kwak, H.; Seo, D. H.; Kim, J.; Jung, Y. S. $NaAlCl_4$: new halide solid electrolyte for 3 V stable cost-effective all-solid-state Na-ion batteries. *ACS Energy Lett.* **2022**, *7* (10), 3293−3301.
(32) Lin, X.; Zhao, Y.; Wang, C.; Luo, J.; Fu, J.; Xiao, B.; Gao, Y.; Li, W.; Zhang, S.; Xu, J.; et al. A Dual Anion Chemistry-Based Superionic Glass Enabling Long-Cycling All-Solid-State Sodium-Ion Batteries. *Angew. Chem., Int. Ed.* **2024**, *63* (2), No. e202314181.
(33) Li, X.; Xu, Y.; Zhao, C.; Wu, D.; Wang, L.; Zheng, M.; Han, X.; Zhang, S.; Yue, J.; Xiao, B.; et al. The Universal Super Cation-Conductivity in Multiple-Cation Mixed Chloride Solid-State Electrolytes. *Angew. Chem., Int. Ed.* **2023**, *62* (48), No. e202306433.
(34) Wei, Z.; Nazar, L. F.; Janek, J. Emerging Halide Solid Electrolytes for Sodium Solid-State Batteries: Structure, Conductivity, Paradigm of Applications. *Batter. Supercaps* **2024**, *7*, No. e202400005.
(35) Dai, T.; Wu, S.; Lu, Y.; Yang, Y.; Liu, Y.; Chang, C.; Rong, X.; Xiao, R.; Zhao, J.; Liu, Y.; et al. Inorganic Glass Electrolytes with Polymer-like Viscoelasticity. *Nat. Energy* **2023**, *8* (11), 1221−1228.
(36) Rodrigues, M. T. F.; Shkrob, I. A.; Colclasure, A. M.; Abraham, D. P. Fast Charging of Li-Ion Cells: Part IV. Temperature Effects and "Safe Lines" to Avoid Lithium Plating. *J. Electrochem. Soc.* **2020**, *167* (13), 130508.
(37) Huang, S.; Wu, X.; Cavalheiro, G. M.; Du, X.; Liu, B.; Du, Z.; Zhang, G. In Situ Measurement of Lithium-Ion Cell Internal Temperatures during Extreme Fast Charging. *J. Electrochem. Soc.* **2019**, *166* (14), A3254.
(38) Wang, C. Y.; Liu, T.; Yang, X. G.; Ge, S.; Stanley, N. V.; Rountree, E. S.; Leng, Y.; McCarthy, B. D. Fast Charging of Energy-Dense Lithium-Ion Batteries. *Nature* **2022**, *611* (7936), 485−490.
(39) Yang, X. G.; Liu, T.; Gao, Y.; Ge, S.; Leng, Y.; Wang, D.; Wang, C. Y. Asymmetric Temperature Modulation for Extreme Fast Charging of Lithium-Ion Batteries. *Joule* **2019**, *3* (12), 3002−3019.
(40) Singh, B.; Wang, Y.; Liu, J.; Bazak, J. D.; Shyamsunder, A.; Nazar, L. F. The Critical Role of Framework Flexibility and Disorder in Driving High Ionic Conductivity in $LiNbOCl_4$. *J. Am. Chem. Soc.* **2024**, *146* (25), 17158−17169.
(41) Harris, R. K.; Nesbitt, G. J. Cross Polarization for Quadrupolar Nuclei−Proton to Sodium-23. *J. Magn. Res. (1969)* **1988**, *78* (2), 245−256.
(42) Bain, A. D. Chemical Exchange in NMR. *Prog. Nucl. Magn. Reson. Spectrosc.* **2003**, *43* (3−4), 63−103.
(43) George, A. M.; Stebbins, J. F. Dynamics of Na in Sodium Aluminosilicate Glasses and Liquids. *Phys. Chem. Miner.* **1996**, *23* (8), 526−534.
(44) Li, Y.; Deng, Z.; Peng, J.; Chen, E.; Yu, Y.; Li, X.; Luo, J.; Huang, Y.; Zhu, J.; Fang, C.; et al. A P2-Type Layered Superionic Conductor Ga-Doped $Na_2Zn_2TeO_6$ for All-Solid-State Sodium-Ion Batteries. *Chem. Eur. J.* **2018**, *24* (5), 1057−1061.
(45) Inglis, K. K.; Corley, J. P.; Florian, P.; Cabana, J.; Bayliss, R. D.; Blanc, F. Structure and Sodium Ion Dynamics in Sodium Strontium Silicate Investigated by Multinuclear Solid-State NMR. *Chem. Mater.* **2016**, *28* (11), 3850−3861.

https://doi.org/10.1021/acsenergylett.4c01855
ACS Energy Lett. 2024, 9, 4093−4101

(46) Yu, C.; Ganapathy, S.; de Klerk, N. J. J.; van Eck, E. R. H.; Wagemaker, M. Na-Ion Dynamics in Tetragonal and Cubic Na_3PS_4, a Na-Ion Conductor for Solid State Na-Ion Batteries. *J. Mater. Chem. A* **2016**, *4* (39), 15095−15105.
(47) Zhou, L.; Bazak, J. D.; Singh, B.; Li, C.; Assoud, A.; Washton, N. M.; Murugesan, V.; Nazar, L. F. A New Sodium Thioborate Fast Ion Conductor: $Na_3B_5S_9$. *Angew. Chem., Int. Ed.* **2023**, *62* (30), No. e202300404.
(48) Kaus, M.; Guin, M.; Yavuz, M.; Knapp, M.; Tietz, F.; Guillon, O.; Ehrenberg, H.; Indris, S. Fast Na^+ Ion Conduction in NASICON-Type $Na_{3.4}Sc_2(SiO_4)_{0.4}(PO_4)_{2.6}$ Observed by ^{23}Na NMR Relaxometry. *J. Phys. Chem. C* **2017**, *121* (3), 1449−1454.
(49) Huang, Y.; Yan, Z.; Luo, W.; Hu, Z.; Liu, G.; Zhang, L.; Yang, X.; Ou, M.; Liu, W.; Huang, L. Vitalization of P2−$Na_{2/3}Ni_{1/3}Mn_{2/3}O_2$ at High-Voltage Cyclability via Combined Structural Modulation for Sodium-Ion Batteries. *Energy Storage Mater.* **2020**, *29*, 182−189.
(50) Wang, L.; Sun, Y. G.; Hu, L. L.; Piao, J. Y.; Guo, J.; Manthiram, A.; Ma, J.; Cao, A. M. Copper-Substituted $Na_{0.67}Ni_{0.3-x}Cu_xMn_{0.7}O_2$ Cathode Materials for Sodium-Ion Batteries with Suppressed P2−O2 Phase Transition. *J. Mater. Chem. A* **2017**, *5* (18), 8752−8761.
(51) Liu, Q.; Hu, Z.; Chen, M.; Zou, C.; Jin, H.; Wang, S.; Gu, Q.; Chou, S. P2-Type $Na_{2/3}Ni_{1/3}Mn_{2/3}O_2$ as a Cathode Material with High-Rate and Long-Life for Sodium Ion Storage. *J. Mater. Chem. A* **2019**, *7* (15), 9215−9221.
(52) Lee, D. H.; Xu, J.; Meng, Y. S. An Advanced Cathode for Na-Ion Batteries with High Rate and Excellent Structural Stability. *Phys. Chem. Chem. Phys.* **2013**, *15* (9), 3304−3312.
(53) Li, Z.; Ding, J.; Mitlin, D. Tin and Tin Compounds for Sodium Ion Battery Anodes: Phase Transformations and Performance. *Acc. Chem. Res.* **2015**, *48* (6), 1657−1665.
(54) Zhou, L.; Zuo, T.; Li, C.; Zhang, Q.; Janek, J.; Nazar, L. F. $Li_{3-x}Zr_x(Ho/Lu)_{1-x}Cl_6$ Solid Electrolytes Enable Ultrahigh-Loading Solid-State Batteries with a Prelithiated Si Anode. *ACS Energy Lett.* **2023**, *8* (7), 3102−3111.
(55) Zhang, W.; Weber, D. A.; Weigand, H.; Arlt, T.; Manke, I.; Schröder, D.; Koerver, R.; Leichtweiss, T.; Hartmann, P.; Zeier, W. G.; et al. Interfacial Processes and Influence of Composite Cathode Microstructure Controlling the Performance of All-Solid-State Lithium Batteries. *ACS Appl. Mater. Interfaces* **2017**, *9* (21), 17835−17845.
(56) Mao, J.; Liu, X.; Liu, J.; Jiang, H.; Zhang, T.; Shao, G.; Ai, G.; Mao, W.; Feng, Y.; Yang, W.; et al. P2-Type $Na_{2/3}Ni_{1/3}Mn_{2/3}O_2$ Cathode Material with Excellent Rate and Cycling Performance for Sodium-Ion Batteries. *J. Electrochem. Soc.* **2019**, *166* (16), A3980.
(57) Song, Z.; Wang, T.; Yang, H.; Kan, W. H.; Chen, Y.; Yu, Q.; Wang, L.; Zhang, Y.; Dai, Y.; Chen, H.; et al. Promoting High-Voltage Stability through Local Lattice Distortion of Halide Solid Electrolytes. *Nat. Commun.* **2024**, *15* (1), 1481.
(58) Ahuis, M.; Doose, S.; Vogt, D.; Michalowski, P.; Zellmer, S.; Kwade, A. Recycling of Solid-State Batteries. *Nat. Energy* **2024**, *9* (4), 373−385.

https://doi.org/10.1021/acsenergylett.4c01855
ACS Energy Lett. 2024, 9, 4093−4101